AIAA JOURNAL
Vol. 42, No. 8, August 2004

Rapid Preliminary Design of Rectangular Linear Cellular Alloys for Maximum Heat Transfer

Rajesh S. Kumar* and David L. McDowell†
Georgia Institute of Technology, Atlanta, Georgia 30332-0405

Design has traditionally involved selecting a suitable material for a given application. An understanding of structure–property relationships provides a more rigorous and scientific basis for choosing an appropriate material for a given set of performance requirements. Improved designs may be possible if the material microstructures could be tailored for application-specific performance requirement. Honeycombs, two-dimensional prismatic cellular metals extended in the third direction, are emerging as an important material system for multifunctional applications. A specific example of designing prismatic cellular microstructure of rectangular cell topology is considered for optimum heat transfer via forced convection through its cells. As opposed to most existing designs, which assume uniform cell structures a priori, grading the cell structure is considered to achieve optimal heat transfer performance. A two-dimensional finite element methodology is developed to model convective heat transfer through a rectangular cellular structure in an approximate yet efficient way, enabling rapid exploration of the design space for purposes of preliminary design. Novel features of the finite element methodology are that it models the void and convection heat transfer due to fluid flow through it in an implicit manner and that it employs sink terms in the energy equation to address heat transfer due to convection down the length of the cells, employing an isothermal upper bound solution strategy for each cell. The finite element approach is used in conjunction with optimization algorithms to design uniform and graded rectangular cell structures.

Introduction

IT is well known that the hierarchy of structural features and mechanisms at different spatial and temporal scales control the properties of materials. Much effort in the materials community has been devoted to establishing structure–property relationships. Understanding these relationships and mechanisms of deformation and fracture has provided a more scientific basis for choosing an appropriate material for a given application. However, when one views the material as an integral part of the design process, the paradigm changes from material selection to material design. Olson[1] has argued for a materials design philosophy rooted in Cohen's reciprocity argument[2] that material microstructure may be considered as being controlled by the property requirements. Simply stated, the goal of materials design is to tailor the microstructure of materials to satisfy performance objectives, subject to constraints on processing, joining, cycle time, cost, etc.

In the past decade, cellular metals have emerged as promising multifunctional material systems. Cellular metals have a combination of properties that make them suitable for a range of applications such as ultralight structures, heat exchangers, fuel cell and battery subsystems, energy absorption systems, vibration control, and acoustical scattering.[3,4] In many applications, the material is required to meet multiple performance objectives. For example, it may be required to carry mechanical loads as well as to serve as a heat dissipation medium.

Two kinds of cellular materials are common: stochastic foams and ordered materials. Stochastic foams consist of randomly distributed open and/or closed cells. On the other hand, ordered materials may be classified as either lattice block materials or prismatic materials. Lattice block materials are planar or spatial arrangements of one-dimensional bars, whereas prismatic materials consist of the assembly of cells in the plane with channels running in the out-of-plane direction, for example, honeycombs. A somewhat less common type of prismatic material is one with graded cell sizes or shapes in the plane, extended prismatically in the third direction. Such structures may have short- or long-range order in the plane, or may be disordered in the plane. Properties of prismatic and stochastic cellular materials are fairly well documented,[3,4] and increasing attention is being devoted to lattice materials.[5–8]

In aerospace structures, stochastic foams and hexagonal honeycombs have been used as the core of sandwich structures. In sandwich structures, these materials play a secondary role of bonding the two face sheets. However, with better understanding, characterization, and design, cellular materials can be used in primary structural systems of an aerospace vehicle. For example, prismatic cellular materials can be integrated with the skin or stringers of an aerospace vehicle to provide active cooling. These materials can also be tailored to provide structural stiffness and strength characteristics in addition to their heat transfer capability.

Because cellular metals have potential for multifunctional applications, researchers are developing guidelines for design using these materials.[4,9–11] These studies have focused on comparing properties of stochastic foams and prismatic materials of different cell shapes such as square, triangular, and hexagonal. The design strategy advocated in these works is based on selecting a suitable uniform cell structure and size for a given application. A particular cell structure is often chosen based on intuition and is then analyzed to obtain a performance index that is representative of a given application. For example, stiffness, strength, heat dissipation, and weight indices have been developed for various prismatic cellular structures and stochastic foams. Crossplots of these indices are obtained for different cellular materials, and the most appropriate one is chosen for a given performance specification. For multifunctional requirements, two or more of these indices are judiciously combined to provide a single index. For example, to assess different prismatic cellular metals for combined thermal and structural performance, Gu et al.[10] and Evans et al.[11] defined a peak thermomechanical index as a multiplicative combination of structural and maximum thermal performance indices. These notions essentially extend the methods of Ashby et al. for materials selection to the realm of materials design.[4]

Although the current design strategy for cellular materials is of considerable practical value in choosing an appropriate structure for

Presented as Paper 2002-5569 at the AIAA/ISSMO 9th Symposium on Multidisciplinary Analysis and Optimization, Atlanta, GA, 5–6 September 2002; received 2 April 2003; revision received 18 March 2004; accepted for publication 30 March 2004.

*Postdoctoral Fellow, G. W. Woodruff School of Mechanical Engineering.
†Professor, G. W. Woodruff School of Mechanical Engineering; David.McDowell@me.getech.edu.

a given application, it severely restricts one's choices to cell topologies that are currently available and well characterized. For example, numerous possibilities are ignored that might combine two or more different cell types and graded cell sizes; these might yield an optimum or near-optimum design for a given multifunctional objective, as suggested by graded topologies that are ubiquitous in nature.

In the present paper, we consider the microstructure design of prismatic or honeycomb cellular metals [also referred to herein as linear cellular alloys (LCAs)] for a given performance requirement, namely, maximum heat transfer due to forced convection. LCAs are manufactured using powder extrusion processes developed by Cochran et al.[12] With this technique, complex cell geometries can be realized. Microstructural variations in these materials are described to lie within a plane, which facilitates tractable design exploration. Prismatic cellular materials such as LCAs offer a rich problem set in which to develop the principles of designing multifunctional materials.

In contrast to most existing designs that consider uniform cell structures, we allow the cells to be nonuniform and functionally graded, thereby endowing more freedom to obtain an optimum or near-optimum design. However, we restrict ourselves in this paper to rectangular cell topology, leaving design of other topologies as well as that of functionally gradient topology to future works. Because the most time-consuming aspect of the present design problem is the analysis step, we introduce an efficient homogenization-based finite element approach for convective heat transfer analysis of LCAs. In this approach, the out-of-plane convective heat transfer process is modeled implicitly as distributed heat sinks in the two-dimensional domain. This two-dimensional analysis procedure is based on certain approximate simplifying assumptions regarding the out-of-plane convective processes. However, it facilitates rapid exploration of the design space of cellular geometry for purposes of preliminary design. The performance of the design obtained using this approach can be assessed and further refined/optimized in the neighborhood of interesting extrema of the objective function using more rigorous three-dimensional analyses based, for example, on computational fluid dynamics codes.

The paper is organized as follows: First we describe the design problem and the geometry under consideration. The finite element formulation of the analysis procedure and its validation are discussed next. This is followed by a discussion of the optimization procedure. Finally, we present the resulting optimum designs, followed by conclusions.

Design Problem for LCAs

Any single- or multi-objective optimization problem can be cast into the following standard mathematical form: Minimize the objective functions

$$f_r(x_i), \qquad i = 1, \ldots, n, \qquad r = 1, \ldots, R \tag{1}$$

such that the following constraints and bounds are satisfied.

Equality constraints:

$$h_j(x_i) = 0, \qquad j = 1, 2, \ldots, n_h \tag{2}$$

Inequality constraints:

$$g_k(x_i) \le 0, \qquad k = 1, 2, \ldots, n_g \tag{3}$$

Bounds on design variables:

$$x_i^l \le x_i \le x_i^u, \qquad i = 1, 2, \ldots, n \tag{4}$$

where we have n design variables x_i, R objective functions, n_h equality constraints, and n_g inequality constraints. Furthermore, the design variables are each constrained by a lower bound x_i^l and an upper bound x_i^u. For single-objective optimization problems, $R = 1$.

For LCAs, a range of design problems involving mechanical, thermal, electrical, and acoustical properties may be formulated, depending on the application. In multifunctional applications, either a single-objective function, defined as a weighted combination of different objectives, or multiple-objective functions may be introduced. When different objectives are treated separately, that is, as a vector in the optimization process, a Pareto optimal solution set may be obtained (see Ref. 13). All solutions in this set are optimal, that is, no solution from this set can be claimed as better than the others. A particular solution from this set is chosen based on (usually qualitative) higher level information from the user.[13] In some cases, it may be convenient to choose a dominant property to form the basis for an objective function and the remaining properties involved as constraints.

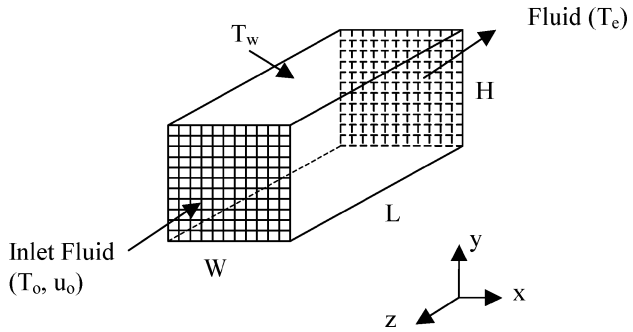

Fig. 1 Geometry considered for design.

In the present paper, we are concerned with designing a rectangular cell LCA for maximum heat transfer via forced convection. A schematic of the geometry is shown in Fig. 1. The overall dimensions of the LCA, length L, width W, and height H, are considered as fixed parameters. The inlet air is pumped at room temperature T_0 with a uniform velocity u_0 in the z direction. Two different boundary conditions are considered: 1) The top surface is held at a constant uniform temperature T_w while the remaining sides are assumed to be insulated. 2) Both the top and the bottom surface are held at constant (but different) uniform temperature, with the remaining sides insulated. The total mass flow rate through the system is $\dot{m}_0$. The aim is to design a microstructure, generally nonuniform, composed of rectangular cells in the x–y plane such that the total steady-state convective heat transfer rate (in the z direction) is maximized.

Approach

The approach adopted for designing rectangular cells for maximum convective heat transfer is inspired by the topology optimization method.[14–19] However, the present approach differs from conventional topology optimization. In the standard formulation of the topology optimization, the domain is discretized into a number of finite elements. The elements are assumed to be composed of a porous material with a density parameter that is allowed to vary continuously between zero and one. The final design is forced to be a zero–one design, with zero and one representing void and solid, respectively. This is typical of strength or stiffness optimization problems, analyzed using boundary-value problem solutions that employ local constitutive equations.

In the present problem, we are interested in distributing solid and void phases in a plane with convective flow occurring in the out-of-plane direction through the void. The effect of convective heat flow must be taken into account while still performing an otherwise two-dimensional analysis of material distribution in the x–y plane. The scalar density parameter cannot be used to define the microstructure within an element because the convective heat transfer and pressure drop within a cell depends on shape, as well as size of the void in the element. There is a length scale associated with the convection process because it depends on the surface area to volume ratio of a cell. Furthermore, the procedure of forcing an element with a small void to be a fully dense solid, as adopted in conventional topology optimization, cannot be used because such an element might be convecting a significant amount of heat if it is near the heat source: Forcing it to be a fully dense solid would limit it to zero convective heat transfer.

In the present case of designing a cellular structure with only rectangular cells, the overall rectangular domain is divided into

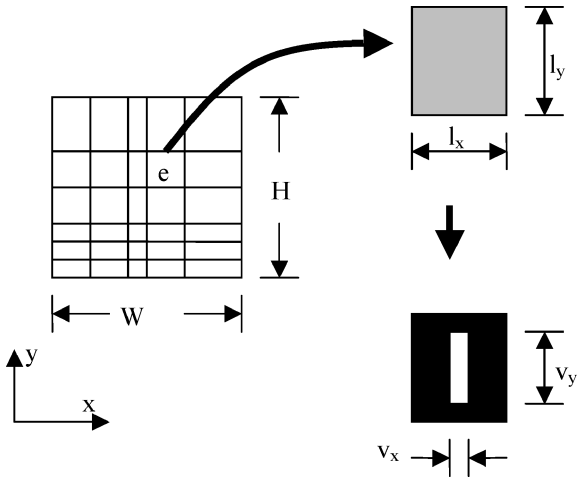

Fig. 2 Discretization of the domain and the cell structure associated with elements.

rectangular elements. Furthermore, each element is associated with exactly one rectangular cell. The rectangular cell associated with the element is not modeled explicitly at the element level. The effect of rectangular cell and the convection heat transfer through it is modeled via temperature-dependent sink (Fig. 2). The sink strength is determined by solving a micromechanics problem of laminar flow through a rectangular duct as explained later. This approach is different than the one adopted by Seepersad et al.,[20] where, at each iteration of the optimization procedure, the three-dimensional convection heat transfer through the cellular structure is explicitly solved using a finite difference approach. The equivalent homogenized modeling of the convection through the cells, as adopted in the present paper, reduces the computation time and can be extended to a more general continuum field approach; such an approach would involve associating a number of cells with each element. The continuum field approach would be suitable for problems where the domain size is much larger than the cell size so that the behavior of a material point (e.g., integration point in a finite element model) is governed by variables characterizing the cell topology associated with that material point. Furthermore, in a continuum field approach, the final discrete topology will have to be obtained from the continuous field solutions using some sort of reconstruction procedure. For the present problem, however, the domain size is of the same order as the cell size, and hence, we associate each element with exactly one cell. This also renders the postprocessing step trivial. The details of the analysis and optimization procedures are outlined in the following subsections.

Analysis Procedure

The configuration shown in Fig. 1 must be analyzed to obtain the total steady-state heat transfer rate in the z direction for different cell structures assigned in the x–y plane. We restrict the fluid flow to be laminar and fully developed, which is justified because the length L is usually much larger than the cell diameter. As already discussed, we consider the domain as continuous with the effect of rectangular voids modeled implicitly. The analysis is restricted to the x–y plane with the effect of convective heat flow through the voids (in the z direction) modeled using distributed sinks. These sinks account for the convective heat transfer through the voids, and their strength depends on the void size and shape, out-of-plane length of the domain, fluid properties, and local temperature of the void surface. In the following subsection, we develop a two-dimensional finite element method incorporating distributed sinks.

Finite Element Formulation with Distributed Sinks

Consider a two-dimensional domain Ω with boundary $\partial\Omega$. Let $\partial\Omega = \partial\Omega_g \cup \partial\Omega_h$ (with $\partial\Omega_g \cap \partial\Omega_h = \phi$), where $\partial\Omega_g$ is the part of the boundary where the Dirichlet boundary condition (temperature) is prescribed and $\partial\Omega_h$ is the part of the boundary where the Neumann boundary condition (heat flux) is prescribed. Heat conduction in Ω is assumed to occur in the x–y plane. Furthermore, we assume that the domain has a continuous distribution of source, $Q(x, y)$ [and, hence, sinks $-Q(x, y)$]. The sinks are introduced to model the out-of-plane convection of heat from the LCA to the fluid as discussed earlier.

The strong forms of the governing equations for the steady-state heat transfer problem are given by[21]

$$\nabla \cdot (\boldsymbol{D} \cdot \nabla T) + Q = 0 \qquad \text{in} \quad \Omega \tag{5}$$

$$q_n = \boldsymbol{q} \cdot \boldsymbol{n} = h \qquad \text{on} \quad \partial\Omega_h \tag{6}$$

$$T = g \qquad \text{on} \quad \partial\Omega_g \tag{7}$$

where $\boldsymbol{D}$ is the effective conductivity tensor, T is the temperature field, $\boldsymbol{q}$ is the heat flux vector, $\boldsymbol{n}$ is the unit normal vector, h is the magnitude of the specified normal flux on the boundary, and g is the specified temperature. Following the standard procedure, the strong form can be converted into the weak form, that is,

$$\int_\Omega (\nabla v)^T \cdot \boldsymbol{D} \cdot \nabla T \, \mathrm{d}A = -\int_{\partial\Omega_h} v h \, \mathrm{d}s + \int_\Omega v Q \, \mathrm{d}A \tag{8}$$

where v is the weighting function and the heat source/sink Q is assumed to depend on temperature T in addition to spatial position. In matrix notation, Eq. (8) can be written as

$$\int_\Omega \{\nabla v\}^T [D] \{\nabla T\} \, \mathrm{d}A = -\int_{\partial\Omega_h} v h \, \mathrm{d}s + \int_\Omega v Q \, \mathrm{d}A \tag{9}$$

where

$$\{\nabla T\} = \begin{Bmatrix} \dfrac{\partial T}{\partial x} \\ \dfrac{\partial T}{\partial y} \end{Bmatrix}, \qquad \{\nabla v\} = \begin{Bmatrix} \dfrac{\partial v}{\partial x} \\ \dfrac{\partial v}{\partial y} \end{Bmatrix}, \qquad [D] = \begin{bmatrix} D_{xx} & D_{xy} \\ D_{xy} & D_{yy} \end{bmatrix} \tag{10}$$

Now consider the standard Galerkin finite element approximation. We divide the domain Ω into N subdomains (elements) Ω^e. The temperature and weighting functions within an element are approximated from the nodal temperatures using the element shape functions N^e. Substituting these approximations in Eq. (9) written over an element domain Ω^e, and recognizing that the weighting function is arbitrary, we get

$$\left(\int_{\Omega^e} [B^e]^T [D^e] [B^e] \, \mathrm{d}A \right) \{T^e\} = -\int_{\partial\Omega_h^e} [N^e]^T h^e \, \mathrm{d}s + \int_{\Omega^e} [N^e]^T Q^e \, \mathrm{d}A \tag{11}$$

where $[B^e]$ is a matrix relating the temperature gradient $\{\nabla T\}$ to the nodal temperature $\{T^e\}$ and $[D^e]$ is the effective element conductivity matrix that is a function of underlying void dimensions and solid and fluid conductivities as derived in the next subsection. Equation (11) is in the standard form from which the element stiffness matrix is obtained, using the bracketed terms on the left-hand side, and the load vector is derived from the two terms on the right-hand side. In the standard treatment of heat conduction problems via the finite element method, it is assumed that the heat source is prescribed in the domain and, hence, known. However, in the present formulation, the heat source is not prescribed but rather depends on temperature. This is because convective heat transfer is modeled by a distributed source/sink term that depends on the temperature differential between the solid and the fluid regions, which may vary spatially in the domain. The sink strength in joules per square meter per second is defined as

$$Q = -\alpha_{\text{eff}} (T - T_0) \tag{12}$$

where T_0 is the inlet temperature of the fluid and α_{eff} is the effective convection coefficient that captures the effect of out-of-plane length,

void shape and size, fluid properties, etc. Note that the negative sign arises from modeling the effect as a sink. Returning to the finite element formulation, we define the average sink strength within each element as

$$Q^e = -\alpha^e_{\text{eff}}\left(T^e_{\text{av-void}} - T_0\right) \tag{13}$$

where $T^e_{\text{av-void}}$ is the average temperature on the void surface that is associated with the element. The average void surface temperature within an element is obtained from the nodal temperatures using an appropriate interpolation function. We choose the element shape functions to interpolate the void surface temperature from the element nodal temperatures according to

$$T^e_{\text{av-void}} = \left(\frac{1}{\partial\Omega^e_{\text{void}}}\int_{\partial\Omega^e_{\text{void}}}[N^e]\,\mathrm{d}A\right)\{T^e\} = [R^e]\{T^e\} \tag{14}$$

The element effective in-plane convection coefficient, α^e_{eff}, is obtained by solving a micromechanics problem of laminar flow through a rectangular duct, as discussed later. Equation (13) can now be written as

$$Q^e = -\alpha^e_{\text{eff}}([R^e]\{T^e\} - T_0) \tag{15}$$

Substituting Eq. (15) into the discretized version of the weak form, Eq. (11), we get

$$\left(\int_{\Omega^e}[B^e]^T[D^e][B^e]\,\mathrm{d}A + \int_{\Omega^e}\alpha^e_{\text{eff}}[N^e]^T[R^e]\,\mathrm{d}A\right)\{T^e\}$$

$$= -\int_{\partial\Omega^e_h}[N^e]^T h^e\,\mathrm{d}s + \int_{\Omega^e}\alpha^e_{\text{eff}}[N^e]^T T_0\,\mathrm{d}A \tag{16}$$

This may be written in compact form as

$$[K^e]\{T^e\} = \{f^e\} \tag{17}$$

Assembly of the elements follows in the usual way to obtain the global equations

$$[K^G]\{T^G\} = \{f^G\} \tag{18}$$

The global (assembled) equations can be solved after imposing the proper boundary conditions. Note that the element stiffness matrix and, hence, the global stiffness matrix are unsymmetric due to the presence of the temperature-dependent sinks/sources in the domain. The finite element formulation, discussed in the foregoing text, is implemented in MATLAB® programming environment.[22]

Determination of Element Effective Conductivity Matrix

The effective conductivity of a homogenized finite element is a function of the underlying microstructure and solid and fluid conductivities. In the present case, we assume the underlying microstructure to be a rectangular void of dimensions v^e_x and v^e_y in an element of dimensions l^e_x and l^e_y in the x and y directions, respectively (Fig. 2). The effective conductivity of the homogenized element, to first order, is obtained by solving one-dimensional conduction equations for equivalent thermal circuits in the x and y directions.[23] When isotropic conductivities for solid (k_s) and fluid (k_f) phases are assumed, and any contact resistance between the solid and the fluid is neglected, the effective conductivity matrix is obtained as

$$[D^e] = \begin{bmatrix} D^e_{11} & 0 \\ 0 & D^e_{22} \end{bmatrix} \tag{19}$$

where

$$D^e_{11} = \frac{k_s k_f l^e_x \left(v^e_y\right)^2}{l^e_y\left[k_s v^e_x v^e_y + k_f v^e_y\left(l^e_x - v^e_x\right)\right]} + \frac{k_s\left(l^e_y - v^e_y\right)}{l^e_y} \tag{20}$$

$$D^e_{22} = \frac{k_s k_f l^e_y \left(v^e_x\right)^2}{l^e_x\left[k_s v^e_x v^e_y + k_f v^e_x\left(l^e_y - v^e_y\right)\right]} + \frac{k_s\left(l^e_x - v^e_x\right)}{l^e_x} \tag{21}$$

Note that the overall conductivity is orthotropic due to the underlying rectangular void within the element.

Determination of Element Effective Convection Coefficient

In the present formulation, each element is taken to be rectangular with a rectangular void defining its underlying microstructure. The convective coefficient α^e_{eff} for each element is determined by solving a three-dimensional micromechanics problem of laminar flow through a rectangular duct. The in-plane dimension of the rectangular duct is taken as the void dimension, and its out-of-plane dimension is the same as the heat exchanger length L. It is assumed that the walls of each duct are at constant temperature $T^e_{\text{av}-\text{void}}$, which is the average temperature of the void surface in the x–y plane of the finite element analysis (corresponding to the inlet cross section). In reality, the wall temperature changes along the length of the duct due to out-of-plane conduction and convection processes. The isothermal assumption yields an upper bound solution to the total heat transfer rate: As long as it provides a consistent and monotonic relation with the total heat transfer rate as determined from full three-dimensional calculations, we submit that this approximation should suffice for the design of in-plane cell structures. Using the standard energy balance for a rectangular duct with constant wall temperature,[23,24] we obtain the total heat transfer rate in the z direction through an element as

$$Q^e_T = -\dot{m}^e c_p\left[1 - \exp\left(-\alpha^e P^e L/\dot{m}^e c_p\right)\right]\left(T^e_{\text{av}-\text{void}} - T_0\right) \tag{22}$$

where $\dot{m}^e$ is the mass flow rate through the void associated with the element, c_p is the specific heat of the fluid at constant pressure, L is the length of the duct, P^e is the flow perimeter of the void, and T_0 is the inlet temperature of the fluid. The negative sign is used to be consistent with the finite element formulation because the sink strength is considered negative. The laminar flow convection coefficient α^e is related to the fluid conductivity k_f, Nusselt number Nu_D, and hydraulic diameter of the void in the element D^e_h, by[23,24]

$$\alpha^e = k_f Nu_D/D^e_h \tag{23}$$

The values of Nusselt number and hydraulic diameter for rectangular ducts are tabulated.[25] For a group of rectangular cells of different sizes and aspect ratios, the mass flow rate in each cell will be different. The distribution of mass flow rate, as well as the total pressure drop, is estimated to first order by simultaneously solving the linear momentum and continuity equations to partition the mass flow rate among cells, assuming the cells are infinitely long compared to cell diameter (Appendix). Application of Eq. (22) based on cell wall temperatures at the inlet cross section is an approximation that neglects a change of temperature gradient across the cross section as a function of length, which is less accurate because the range of sizes and shapes of cell walls increasingly vary within the cross section. Moreover, the use of a single element to represent a single cell is a low-order approximation that is intended to facilitate rapid, efficient exploration of the design space. As discussed in the next subsection, a single-element representation of one cell with varying void aspect ratio is acceptable for preliminary design exploration. The accuracy can be improved by using higher-order shape functions to model the elements if desired.

The convective heat flux through each element (assumed constant) is obtained by dividing the total heat flow due to convection, Q^e_T [Eq. (22)] by the element planar area A^e as

$$Q^e = -\left(\dot{m}^e c_p/A^e\right)\left[1 - \exp\left(-\alpha^e P^e L/\dot{m}^e c_p\right)\right]\left(T^e_{\text{av}-\text{void}} - T_0\right) \tag{24}$$

When Eqs. (13) and (24) are compared, the effective convection coefficient is obtained as

$$\alpha^e_{\text{eff}} = \left(\dot{m}^e c_p/A^e\right)\left[1 - \exp\left(-\alpha^e P^e L/\dot{m}^e c_p\right)\right] \tag{25}$$

Verification of the Finite Element Formulation

The two-dimensional finite element approach presented in the foregoing is an approximate, reduced approach to model three-dimensional convective heat transfer through prismatic cellular materials. As discussed before, it implicitly models the rectangular voids and their convective heat transfer due to duct flow as temperature-dependent heat sinks. The sink strength is calculated based on micromechanics solution of fluid flow through a rectangular channel with the assumption of isothermal cell walls, with the wall temperature the same as the average void temperature at the inlet cross section. With this assumption, the fluid temperature changes exponentially in the out-of-plane direction [cf., Eq. (25)]. This convection process is modeled through the effective convection coefficient in the two-dimensional finite element formulation. The assumption of isothermal walls for determining the effective convection coefficient leads to an upper bound estimate of the total heat transfer rate.[26]

The finite element formulation discussed in the foregoing text is implemented via a four-noded linear element. The average void surface temperature in an element, $T^e_{\text{av}-\text{void}}$, is interpolated from the element nodal temperature [Eq. (14)]. We first validate the accuracy of the average void temperature predicted by using a homogeneous single finite element by comparing it with predictions of an ABAQUS[27] finite element model that explicitly considers the void and uses multiple numbers of elements along the wall thickness.

The problem considered for this comparison is a single cell LCA of unit width and height. The out-of-plane length is 10 units. The width of the rectangular void is 0.25 units, and its height is varied to get simulations for different void aspect ratios (v_y/l_y). Two different boundary conditions (BC) are considered: 1) BC1, where the top surface is kept at a constant and uniform temperature of 100°C and the remaining sides are insulated and 2) BC2, where top and bottom surfaces are at constant uniform temperatures of 100°C and 20°C, respectively, with the remaining sides insulated. These conditions are the same as those used for the design studies. Air at 20°C enters into the cell at a mass flow rate of 0.0037 kg/s. The material properties used are listed in Table 1. The same material properties, BC, and domain dimensions are considered for both the homogeneous single-element and ABAQUS simulations.

In the ABAQUS simulations, the rectangular void is modeled explicitly. Heat transfer via convection is modeled by specifying a convective film coefficient on the void surface. The magnitude of the film coefficient is calculated from the void dimensions and the fluid properties according to

$$\alpha_{\text{sink}} = (\dot{m}c_p/A_{\text{void}})[1 - \exp(-\alpha PL/\dot{m}c_p)] \qquad (26)$$

where A_{void} is the surface area of the void [cf. Eq. (25)], $\dot{m}$ is the mass flow rate through the duct, and P and L are the flow perimeter and the length of the duct, respectively. A typical ABAQUS finite element mesh is shown in Fig. 3.

Note that multiple elements are used in the $x-y$ plane as opposed to just a single finite element as in the homogenized formulation developed in this paper. Furthermore, a three-dimensional model has to be analyzed in ABAQUS even though there are no gradients in the z direction because the convection coefficient can only be specified on a surface and not on a line. In Table 2, the average temperature on the void surface from ABAQUS simulations is compared with the homogenized solutions for different void aspect ratios.

It is observed that, for both the cases considered, the error increases as the void dimension becomes small compared to the element dimension, as expected. The maximum error is 2.4% for the first case and 0.78% for the second. These are relatively small, which shows that the two-dimensional approximation is adequate for representing three-dimensional analyses of a single cell with more elements subject to the same assumption of isothermal walls down the length of the cell.

To illustrate the upper bound nature of the total heat transfer rate as predicted by the finite element approach and to determine whether the present two-dimensional approximation may be adequate for purposes of preliminary design of a cellular cross section, we compare the total heat transfer rate obtained using this approach with a three-dimensional finite difference code. The finite difference methodology developed for LCAs has been adequately validated with experiments and computational fluid dynamics codes by Dempsey[28] (also see Seepersad et al.[20]). Again we consider an LCA with overall dimension of 0.025×0.025 m in the $x-y$ plane and 0.050 m in the z direction. The fluid is taken to be air at 20°C with a mass flow rate of 0.0037 kg/s. A uniform temperature of 100°C is applied on the top surface with the remaining sides insulated. The material properties are given in Table 1. We consider a range of uniform and graded cell structures for this comparison. Both the horizontal and vertical cell walls are taken to be 150 μm in thickness. The number of cells in the x direction is fixed at 14. For a uniform cell structure, we vary the number of cells in the y direction from 2 to 6. The total heat transfer rate from the present two-dimensional finite element calculations are compared with the three-dimensional finite difference calculations in Table 3. For graded cell structures, we consider 14×2 cell topology. The cells are considered to be

Table 1 Solid and fluid (air at 20°C) properties used in simulations

Property	Value
Fluid conductivity k_f	0.027 W/m · K
Fluid density ρ_f	1.195 kg/m^3
Fluid kinematic viscosity η_f	15.15×10^{-6} m^2/s
Fluid specific heat at constant pressure c_p	1002.7 J/kg · K
Solid conductivity k_s	362 W/m · K

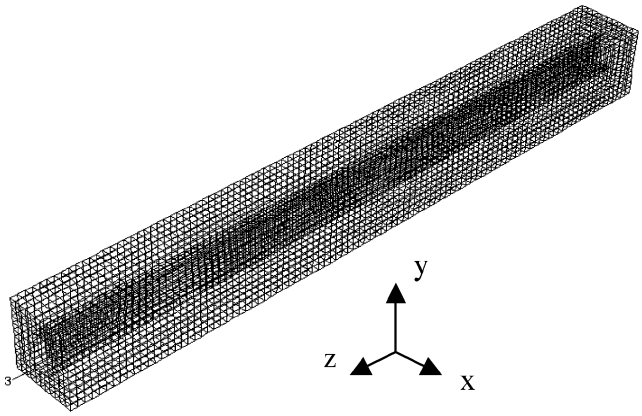

Fig. 3 Typical finite element mesh for ABAQUS simulation, $v_y/l_y = 0.5$.

Table 2 Average void surface temperature from homogenized and ABAQUS simulations of explicit ducts

	BC1, K			BC2, K		
v_y/l_y	Homogeneous	ABAQUS	Error, %	Homogeneous	ABAQUS	Error, %
0.10	372.80	364.07	2.40	333.00	330.43	0.78
0.25	372.84	369.05	1.03	333.00	332.03	0.29
0.50	372.82	369.81	0.81	333.00	332.41	0.18
0.75	372.79	369.89	0.78	333.00	332.51	0.15
0.90	372.77	369.90	0.78	333.00	332.60	0.12

Table 3 Two-dimensional finite element and three-dimensional finite difference solutions for various uniform cell structures

Cell configuration (cell in x, cell in y)	Total heat transfer rate, W		
	Finite element	Finite difference	Error, %
14×2	122.38	98.85	23.8
14×3	120.30	96.27	24.9
14×4	119.39	95.76	24.7
14×5	120.46	96.57	24.7
14×6	123.01	98.33	25.1

Table 4 Two-dimensional finite element and three-dimensional finite difference solutions for various graded cell structures[a]

Ratio of vertical void lengths of the two rows ($v_y^{\text{Row1}}/v_y^{\text{Row2}}$)	Total heat transfer rate, W		
	Finite element	Finite difference	Error, %
0.10	123.16	100.25	22.8
0.24	122.48	97.91	25.1
0.42	122.32	97.29	25.7
1.00	122.87	98.05	25.3
2.37	122.38	98.85	23.8
4.14	122.54	99.68	22.9
9.79	123.19	101.45	21.4

[a]Number of cells along $x = 14$; number of cells along $y = 2$.

uniform in the x direction because no gradients are expected in that direction. For various graded geometries in the y direction, the total heat transfer rate obtained from the finite element and finite difference calculations are compared in Table 4.

Note from these results that the two-dimensional homogenized finite element approach presented in this work overpredicts the total heat transfer rate by 20–25%. This is consistent with the upper bound nature of the total heat transfer rate due to the assumption of isothermal cell walls in calculating the effective sink strength. Also note that the results predicted by the finite element method show consistent trends when compared with the three-dimensional finite difference results; in other words, there is a consistent level of error, with the two-dimensional results tracking the trends of increase or decrease with the three-dimensional results. This consistency and monotonicity of relations between the two-dimensional and three-dimensional models lends credibility to the viability of two-dimensional approximate analyses for selecting cell structures in the cross section of prismatic honeycomb heat sinks; the optimum cell configuration obtained using the two-dimensional approach is expected to be similar to that obtained using accurate three-dimensional analysis routines. Hence the proposed finite element methodology is suitable for purposes of designing the cell geometry. Once an optimal design is identified using the proposed two-dimensional approach, the total heat transfer rate can be evaluated and verified via more accurate schemes, such as three-dimensional finite difference or computational fluid dynamics. Another strategy is to use the two-dimensional model to identify rapidly regions of the design space that are near optimal and then exercise more computationally intensive three-dimensional codes to conduct the final optimization search procedures, that is, detail design.

Optimization Procedure

The two-dimensional finite element formulation developed approximates the total steady-state heat transfer rate through a rectangular LCA as a function of the prescribed geometry, BC, and fluid properties. For design studies, suitable design variables and constraint equations must be defined. The rectangular region of dimension W by H is considered as the design domain for purposes of optimization (Fig. 1). This domain is discretized using rectangular elements with linear shape functions as shown in Fig. 2. We assign as parameters M elements in the x direction and N elements in the y direction. In the finite element analysis, each element is regarded as a continuum with the underlying microstructure modeled implicitly (Fig. 2). Different rectangular cell designs can be obtained by varying the dimensions of the finite elements as well as those of the rectangular voids within the cells that serve to duct the fluid flow. Hence, these dimensions (in the normalized form) are chosen as design variables. However, dimensions of elements are not independent in the present design: All elements in a column are simply constrained to have the same width and all elements in a row are constrained to the same height to maintain compatibility between the elements in filling space.

For uniform cell design with fixed-cell-wall thicknesses, a simple graphical optimization technique is utilized based on conducting parametric analyses. However, for graded cell designs, where both cell size and cell wall thicknesses can vary, a mathematical programming-based optimization approach must be used. For the present problem, we have used the fmincon procedure of the MATLAB optimization toolbox.[29] This procedure uses a sequential quadratic programming to solve the constrained minimization problem. The objective function, design variables, and the constraints used are listed next.

Objective Function

The objective function is defined as the total steady-state heat transfer rate to the fluid across the entire cross section, equal to the sum of the steady-state heat transfer rate from individual cells down the length in the z direction.

Design Variables

In general, for general topological design, element dimensions in the x and y directions, as well as void dimensions in each element, may be taken as design variables. However, to reduce variables for purposes of a simple exercise and to maintain mesh compatibility, all elements in a column are prescribed to have the same x dimension and all elements in a row are prescribed to have same y dimension. Thus, the following design variables are defined: 1) element dimension in the x direction normalized by domain width, $\boldsymbol{d}_1 = l_x^e/W$; 2) element dimension in the y direction normalized by domain height, $\boldsymbol{d}_2 = l_y^e/H$; 3) void dimension in the x direction normalized by the corresponding element dimension, $\boldsymbol{d}_3 = v_x^e/l_x^e$; and 4) void dimension in the y direction normalized by the corresponding element dimension, $\boldsymbol{d}_4 = v_y^e/l_y^e$.

Note that mesh compatibility requires the design vectors $\boldsymbol{d}_1$ and $\boldsymbol{d}_2$ to be specified for only one row and column of the mesh, respectively. Thus, $\boldsymbol{d}_1$ is M by 1 and $\boldsymbol{d}_2$ is N by 1. Void dimensions as a fraction of corresponding element dimensions are defined for each element. Thus, both $\boldsymbol{d}_3$ and $\boldsymbol{d}_4$ are vectors of dimension (MN) by 1.

The preceding set of design variables may lead to designs with a wide range of cell sizes and distributions that may be expensive to manufacture. Furthermore, unsymmetric designs may result for ostensibly symmetric problems. Thus, further constraints may be provided to address such issues.

The overall geometry and the boundary conditions of the present problem are such that no gradients of cells are expected in the x direction. To enforce a requirement of uniform cells in the x direction, two constraints are needed. First, all elements are constrained to have the same x dimension, thereby eliminating the design vector $\boldsymbol{d}_1$. Second, all elements are assumed to have same void dimension in the x direction, thereby reducing the design vector $\boldsymbol{d}_3$ to a scalar. Finally, void dimensions are constrained such that all voids in a row have the same y direction dimension. This ensures that each column has the same cell gradient in the y direction. Thus, $\boldsymbol{d}_4$ is an N by 1 vector. The total number of design variables is, therefore, $2N + 1$.

Constraints

In general, the following equality constraints must be imposed on the design variables $\boldsymbol{d}_1$ and $\boldsymbol{d}_2$:

$$\sum_{i=1}^{M} (d_1)_i = 1, \qquad \sum_{i=1}^{M} (d_2)_i = 1 \tag{27}$$

These constraints ensure that element lengths in x and y directions sum properly to overall domain width and height, respectively. The first constraint in Eq. (27) is redundant in the present problem because the design vector $\boldsymbol{d}_1$ is eliminated by considering uniform cell size along the x direction.

As the heat transfer analysis is restricted to the laminar flow regime, an inequality constraint is imposed on the maximum Reynolds number Re, that is,

$$\max(Re) \leq 2300 \tag{28}$$

The Reynolds number is calculated for the ith cell using the formula $Re_i = V_i D_i / \eta_f$, where V_i and D_i are the mean velocity and hydraulic diameter of the ith cell, respectively, and η_f is the kinematic viscosity of the fluid. The maximum among all of the cells is taken as the maximum Reynolds number.

An additional inequality constraint on pressure drop is needed, in general, to match the pressure drop vs flow velocity characteristics of the fan used to pump the fluid. In the present study, an upper bound constraint on the pressure drop ΔP (in pascals) is specified as

$$\Delta P \leq 50 \tag{29}$$

The total solid area fraction A_{fs} in the domain is required to be at most 0.5. Thus, the inequality constraint on solid area fraction is specified as

$$0 < A_{fs} \leq 0.5 \tag{30}$$

Furthermore, upper and lower bound constraints must be imposed on all design variables to avoid numerical difficulties as the void area fraction approaches either 0 or 1. Bounds may also be based on the manufacturing limitations on the cell wall thickness and aspect ratio of cell walls.

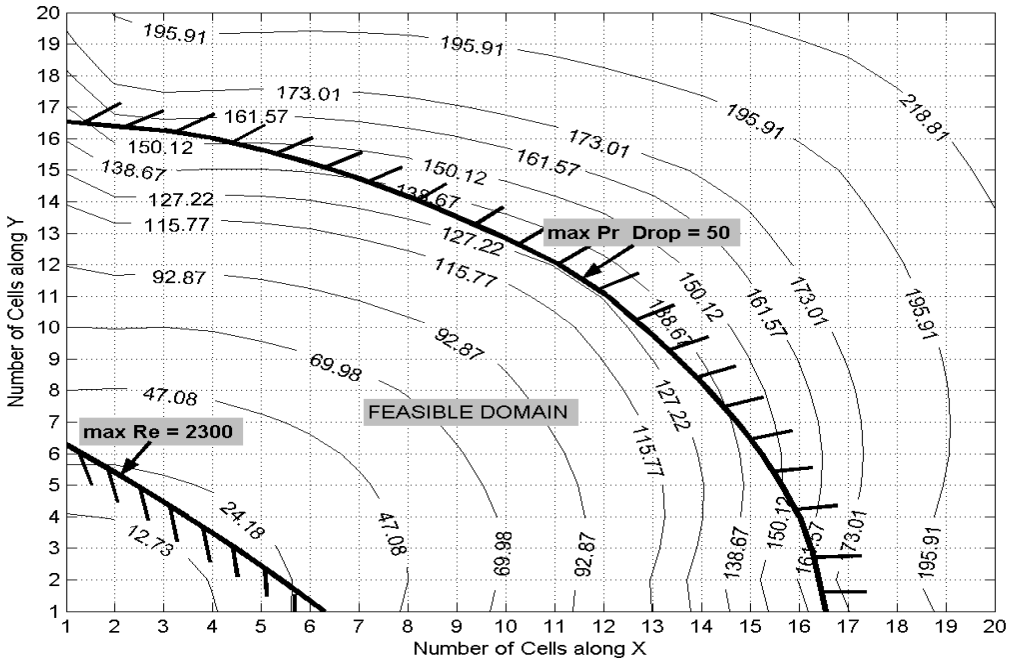

a)

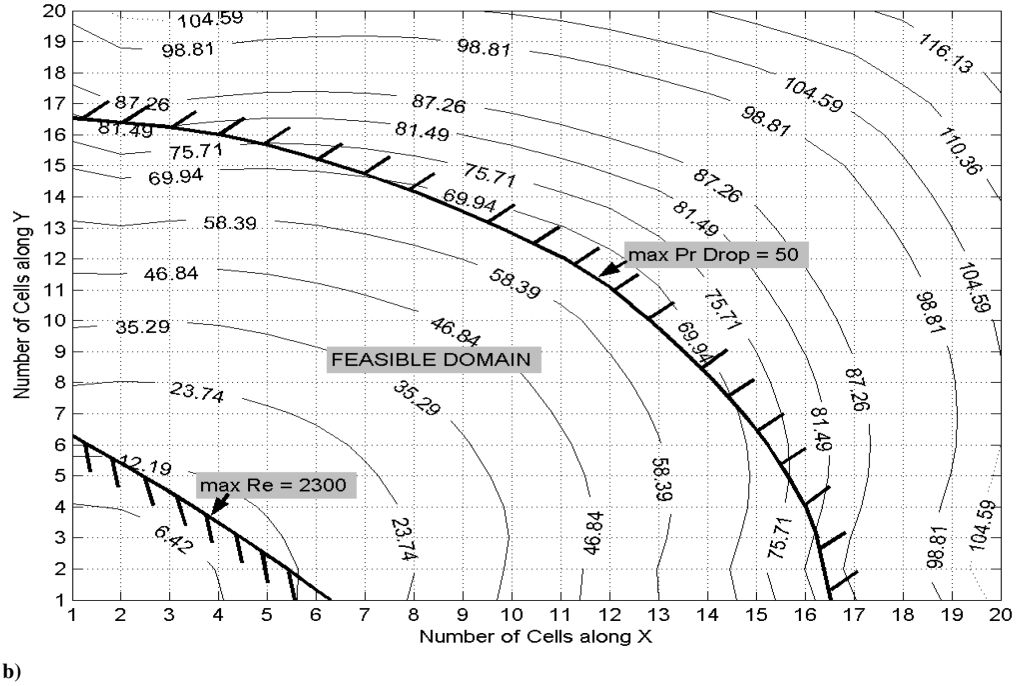

b)

Fig. 4 Contours of total heat transfer rate for various uniform cell structures: a) BC1 and b) BC2.

Results and Discussion

The overall dimensions of the LCA considered in the present study are $W = H = 25$ mm and $L = 50$ mm (Fig. 1). Air at 20°C and with a total mass flow rate of 0.0037 kg/s is taken as the cooling fluid. The relevant fluid and solid properties are listed in Table 1. We consider two different BC: 1) The top surface of the LCA is subjected to uniform temperature of 100° and the remaining lateral surfaces are insulated. 2) The top and bottom surfaces are subjected to uniform temperatures of 100 and 20°C, respectively, and the remaining sides are insulated. We first consider designing uniform cell structures with a specified value of cell wall thickness. Then we consider graded cell designs for which we allow the cell wall thicknesses to vary.

Uniform Cell Designs

In designing a uniform cell structure, a graphical approach to optimization is utilized. The finite element analysis procedure is used to calculate the total steady-state heat transfer rate, pressure drop, and maximum Reynolds number for various combinations of number of cells along the x and y directions. The void dimensions are such that the wall thickness is constant (150 μm for external walls and twice that value for internal walls). The contours of the total heat transfer rate (in watts) for various combinations of number of cells along the x and y directions are shown in Figs. 4a and 4b for the two BC already described. Also shown in Figs. 4 is the contour of pressure drop corresponding to the value of 50 Pa and the contour of maximum Reynolds number corresponding to the value of 2300. The hash marks on these curves indicate the infeasible side. The feasible domain is bounded by these two constraints. All of the designs shown in Fig. 4 have the solid area fraction less than 0.5. From Figs. 4, it is easy to see that for BC 1 the optimum solution corresponds to a 16 by 2 uniform cell structure with the resulting heat transfer rate of approximately 161.6 W. For BC2, the optimum solution again corresponds to a 16 by 2 uniform cell structure with the heat transfer rate of 81.5 W.

Graded Cell Designs

For problems involving strong temperature gradients, graded cell size designs may be more efficient than the uniform ones. In the problem under consideration, we expect nonuniform cell structure along the y direction for efficient heat transfer. In designing such nonuniform structure, we resort to the mathematical programming-based optimization procedure. In the optimization procedure, we allow the thickness of the horizontal and vertical walls to vary. However, we impose that the thickness of the vertical walls be at least 150 μm and at most 500 μm. The thicknesses of the horizontal walls are allowed to vary arbitrarily. We also require that the cell height be at most 0.3 times the domain height. This constraint is imposed to avoid very long thin vertical walls.

A number of optimization runs are conducted with a different number of elements in the x and y directions. The runs were conducted manually although, in principle, they could be automatically executed by a script program. For a selected number of rows and columns, we conduct different runs based on randomly selected initial design guesses. The best solution among all of the trials is chosen as the optimum. Optimal designs obtained considering different numbers of elements in the x and y directions are shown in Fig. 5. Figure 5 also indicates the resulting pressure drop, the maximum Reynolds number, the total heat transfer rates, and the area fraction of solid for each of the resulting design configurations. For a number of cells in the x direction less than 13, we obtained uniform cell structures with 10 cells in the y direction as optimum. However, the total heat transfer rate was considerably less than the 16 by 4 cell structure. Increasing the number of cells in the x direction resulted in the violation of pressure and/or thickness constraint. Thus, the graded 16 by 4 cell structure is the optimum design for the prescribed constraints.

Observe from this design study that the optimum cell structure is only weakly graded. This is to be expected because the temperature gradient in the problem is not significant. Because of the imposed BC (top surface at 100°C and bottom surface insulated), the temperature difference between the top and the bottom surface is not large; typically, 1.0–1.5°C.

To illustrate the utility of a graded cell structure, we consider a different design problem. The geometry, physical properties, etc., are same as the earlier problem. However, the BC are different. We now apply constant uniform temperature of 100°C on the top surface and 20°C on the bottom surface. The remaining two sides are insulated. We vary the number of cells in the x and y directions. The design variables are the element and void dimensions in the y direction. We also impose an upper bound constraint on the vertical dimension of any cell such that the vertical dimension of the cell is at

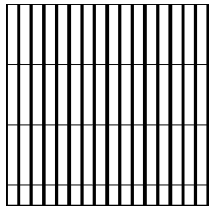

a) 16 × 4 cell structure, total heat transfer rate = 165.19 W, max Re = 899.5, ΔP = 50 Pa, and A_{fs} = 0.2061

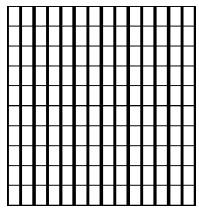

c) 14 × 10 cell structure, total heat transfer rate = 151.11 W, max Re = 739.3, ΔP = 50 Pa, and A_{fs} = 0.1873

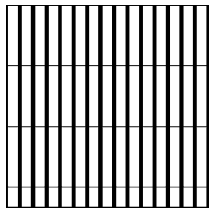

b) 15 × 4 cell structure, total heat transfer rate = 156.26 W, max Re = 957.1, ΔP = 50 Pa, and A_{fs} = 0.2389

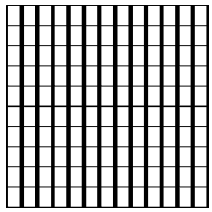

d) 13 × 10 cell structure, total heat transfer rate = 142.18 W, max Re = 787.10, ΔP = 50 Pa, and A_{fs} = 0.2218

Fig. 5 Various optimum cell designs for different number of cells in x and y directions: top surface 100°C, remaining sides insulated.

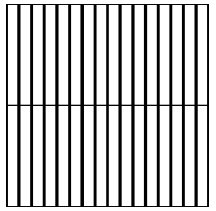

a) 16 × 2 cell structure, total heat transfer rate = 83.81 W, max Re = 939.2, ΔP = 50 Pa, and A_{fs} = 0.2217

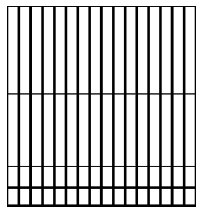

c) 16 × 4 cell structure, total heat transfer rate = 84.07 W, max Re = 1001.6, ΔP = 50 Pa, and A_{fs} = 0.2164

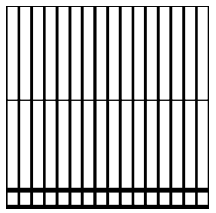

b) 16 × 3 cell structure, total heat transfer rate = 84.15 W, max Re = 995.45, ΔP = 50 Pa, and A_{fs} = 0.2326

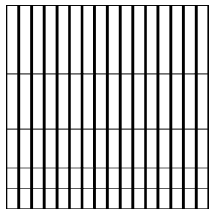

d) 16 × 5 cell structure, total heat transfer rate = 82.95 W, max Re = 963.1, ΔP = 50 Pa, and A_{fs} = 0.2001

Fig. 6 Various optimum cell designs for different number of cells in x and y directions: top surface 100°C, bottom surface 20°C, remaining sides insulated.

most 0.5 times the overall vertical dimension of the LCA. It is found that 16 cells along the x direction leads to optimum heat transfer rate. The resulting cell structures for 16 cells along x direction and varying number of cells along the y direction are shown in Fig. 6. Again, the total heat transfer rate and other relevant quantities are shown in Fig. 6. The optimum cell structure is a graded 16 by 3 arrangement with the total heat transfer rate of 84.2 W. As expected, we see a strongly graded cell structure in this case. Also note that the graded structure results in a higher heat transfer rate than that of the 16 by 2 uniform cell structure.

Conclusions

Designing microstructures for a given set of multifunctional performance objectives and constraints represents a relatively new paradigm for materials design. Such strategies give us an opportunity to tailor the material microstructure to obtain optimal designs. This philosophy is implemented in the present paper toward preliminary design of mesoscopic cell structures of LCAs, which are emerging as an important class of multifunctional materials.

A specific example is considered of designing a rectangular cell LCA heat sink for maximum steady-state heat transfer rate due to forced convection. A two-dimensional finite element formulation is developed for the analysis that models the convective heat flow through temperature-dependent distributed sinks in the domain. The analysis gives an upper-bound solution to the total heat transfer rate and is computationally efficient to facilitate rapid exploration of the design space. Rectangular voids of different size and aspect ratios are distributed in the domain to obtain maximum heat transfer rate subject to a constraint on the maximum pressure drop.

The approach presented though limited to rectangular cell structures, can admit different boundary conditions and can yield uniform and/or graded cell designs. Furthermore, it can be used in conjunction with appropriate structural analysis methods to design for combined mechanical and thermal properties. Further development is needed to generalize the present approach to handle a range of cell shapes simultaneously. This would give the freedom of combining different cell shapes (topology design) in addition to graded designs to enhance performance.

Appendix: Partitioning of Total Mass Flow Rate Among Cells

The cellular mesostructure associated with the design domain evolves during the optimization iteration. At each step, the effective convection coefficient for the homogenized finite element is calculated based on the mass flow rate of the fluid within the rectangular void associated with that element [Eq. (25)]. The overall mass flow rate is partitioned into individual elements (associated voids) by an approximate solution of momentum and continuity equations as described next.

We assume incompressible, isothermal, and laminar flow. Furthermore, we assume that the channels are long compared to the cross-sectional area so that inlet and exit losses are negligible compared to the total pressure drop. We also neglect mechanical boundary-layer effects as well as flow stagnation due to clustering of cells. Let the total mass flow rate be $\dot{m}$. The freestream inlet velocity is given by $V = \dot{m}/(\rho_f A_{\text{total}})$, where A_{total} is the total cross-sectional area of the LCA. The velocity in cell i is defined by

$$V_i = \phi_i V, \qquad i = 1, \ldots, N \tag{A1}$$

where ϕ_i is the velocity scaling factor and N is the total number of cells in the cross section. Total laminar pressure drop, which is same in each cell, is given by

$$\Delta P = \rho_f \xi_i v_f \left(L \Big/ D_i^2\right)(\phi_i V/2) \tag{A2}$$

where ξ_i is the friction factor of the ith cell, L is the out-of-plane length of the channel, and D_i is the hydraulic diameter of the ith cell. From Eq. (A2), we can write

$$\xi_i\left(\phi_i \Big/ D_i^2\right) = \xi_1\left(\phi_1 \Big/ D_1^2\right) = \text{const}, \qquad i = 2, \ldots, N \tag{A3}$$

and, hence,

$$\phi_i = \frac{\mathrm{D}_i^2}{\mathrm{D}_1^2}\frac{\xi_1}{\xi_i}\phi_1, \qquad i = 2, \ldots, N \tag{A4}$$

Now considering the continuity equation (conservation of mass), we can write

$$\rho_f A_{\text{total}} V = \rho_f V \sum_{i=1}^{N} A_i \phi_i \tag{A5}$$

where A_i is the flow area of the ith cell. Substituting Eq. (A4) in Eq. (A5), we obtain

$$\left(A_1 + \sum_{i=2}^{N} A_i \frac{D_i^2}{D_1^2}\frac{\xi_1}{\xi_i}\right)\phi_1 = A_{\text{total}} \tag{A6}$$

For a given collection of cells and fluid properties, Eq. (A6) is solved for the velocity scaling factor of the first cell, ϕ_1. The scaling factors of the remaining cells are then obtained using Eq. (A4). The velocity in each cell is now calculated using Eq. (A1). Finally mass flow rate in each cell is obtained using $\dot{m}_i = \rho_f A_i V_i$.

Acknowledgments

This work is sponsored by Defense Advanced Research Projects Agency/Defense Sciences Office under the Palm Power Program Hybrid Metal/Electrolyte Monolithic Low Temperature SOFCs, Grant DAAD19-01-1-0649, Valerie Browning, Project Director. Support of the Carter N. Paden, Jr. Distinguished Chair in Metals Processing is also gratefully acknowledged.

References

[1]Olson, G. B., "Computational Design of Hierarchically Structured Materials," *Science*, Vol. 277, 1997, pp. 1237–1242.

[2]Cohen, M., "Unknowables in the Essence of Materials Science and Engineering," *Materials Science and Engineering*, Vol. 25, 1976, pp. 3–4.

[3]Gibson, L. J., and Ashby, M. F., *Cellular Solids*, 2nd ed., Cambridge Univ. Press, Cambridge, England, U.K., 1997.

[4]Ashby, M. F., Evans, A. G., Fleck, N. A., Gibson, L. J., Hutchinson, J. W., and Wadley, H. N. G., *Metal Foams: A Design Guide*, Butterworth–Heinemann, Boston, 2000.

[5]Deshpande, V. S., Fleck, N. A., and Ashby, M. F., "Effective Properties of the Octet-truss Lattice Material," *Journal of the Mechanics and Physics of Solids*, Vol. 49, 2001, pp. 1747–1769.

[6]Wallach, J. C., and Gibson, L. J., "Mechanical Behavior of a Three-Dimensional Truss Material," *International Journal of Solids and Structures*, Vol. 38, 2001, pp. 7181–7196.

[7]Wicks, N., and Hutchinson, J. W., "Optimal Truss Plates," *International Journal of Solids and Structures*, Vol. 38, 2001, pp. 5165–5183.

[8]Chiras, S., Mumm, D. R., Evans, A. G., Wicks, N., Hutchinson, J. W., Dharmasena, K., Wadley, H. N. G., and Fichter, S., "The Structural Performance of Near-Optimized Truss Core Panels," *International Journal of Solids and Structures*, Vol. 39, 2002, pp. 4093–4115.

[9]Evans, A. G., Hutchinson, J. W., and Ashby, M. F., "Multifunctionality of Cellular Metal Systems," *Progress in Materials Science*, Vol. 43, 1999, pp. 171–221.

[10]Gu, S., Lu, T. J., and Evans, A. G., "On the Design of Two-Dimensional Cellular Metals for Combined Heat Dissipation and Structural Load Capacity," *International Journal of Heat and Mass Transfer*," Vol. 44, 2001, pp. 2163–2175.

[11]Evans, A. G., Hutchinson, J. W., Fleck, N. A., Ashby, M. F., and Wadley, H. N. G., "The Topological Design of Multifunctional Cellular Metals," *Progress in Materials Science*, Vol. 46, 2001, pp. 309–327.

[12]Cochran, J., Lee, K. J., McDowell, D., Sanders, T., Church, B., Clark, J., Dempsey, B., Hayes, A., Hurysz, K., McCoy, T., Nadler, J., Oh, R., Seay, W., and Shapiro, B., "Low Density Monolithic Metal Honeycombs by Thermal Chemical Processing," *Proceedings of the 4th Conference on Aerospace Materials, Processes and Environmental Technology*, Huntsville, AL, 2000.

[13]Deb, K., *Multi-Objective Optimization using Evolutionary Algorithms*, Wiley, New York, 2001.

[14]Sigmund, O., and Torquato, S., "Composites with Extremal Thermal Expansion Coefficients," *Applied Physics Letters*, Vol 69, 1996, pp. 3203–3205.

[15]Sigmund, O., and Torquato, S., "Design of Materials with Extreme Thermal Expansion Using a Three-Phase Topology Optimization Method," *Journal of the Mechanics and Physics of Solids*, Vol. 45, 1997, pp. 1037–1067.
[16]Bendsoe, M. P., and Kikuchi, N., "Generating Optimal Topologies in Structural Design Using a Homogenization Method," *Computer Methods in Applied Mechanics and Engineering*, Vol. 71, 1988, pp. 197–224.
[17]Eschenauer, H. A., and Olhoff, N., "Topology Optimization of Continuum Structures," *Applied Mechanics Reviews*, Vol. 54, 2001, pp. 331–390.
[18]Hyun, S., and Torquato, S., "Designing Composite Microstructures with Targeted Properties," *Journal of Materials Research*, Vol. 16, 2001, pp. 280–285.
[19]Hyun S., and Torquato, S., "Optimal and Manufacturable Two-dimensional, Kagome-Like Cellular Solids," *Journal of Materials Research*, Vol. 17, 2002, pp. 137–144.
[20]Seepersad, C. C., Dempsey, B. M., Allen, J. K., Mistree, F., and McDowell, D. L., "Design of Mutifunctional Honeycomb Materials," *AIAA Journal*, Vol. 42, No. 5, 2004, pp. 1025–1033.
[21]Ottosen, N., and Petersson, H., *Introduction to the Finite Element Method*, Prentice–Hall, London, 1992.
[22]MATLAB, Ver. 6.5, Release 13, MathWorks, Natick, MA, 2001.
[23]Incropera, F. P., and DeWitt, D. P., *Fundamentals of Heat and Mass Transfer*, 4th ed., Wiley, New York, 1996.
[24]Oosthuizen, P. H., and Naylor, D., *An Introduction to Convective Heat Transfer Analysis*, McGraw–Hill, New York, 1999.
[25]Shah, R. K., and London, A. L., *Laminar Flow Forced Convection in Ducts: A Source Book for Compact Heat Exchanger Analytical Data*, Academic Press, New York, 1978.
[26]Hayes, A. M., Wang, A., Dempsey, B. M., and McDowell, D. L., "Mechanics of Linear Cellular Alloys," *Mechanics of Materials*, Vol. 36, No. 8, 2004, pp. 691–713.
[27]"ABAQUS, User's Manual," *Ver. 6.3-1*, ABAQUS, Inc., Pawtucket, RI, 2002.
[28]Dempsey, B. M., "Thermal Properties of Linear Cellular Alloys," M.S. Thesis, G. W. Woodruff School of Mechanical Engineering, Georgia Inst. of Technology, Atlanta, Aug. 2002.
[29]"Optimization Toolbox—for Use with MATLAB," User's Guide, Ver. 2, MathWorks, Natick, MA, 2001.

K. Shivakumar
Associate Editor